Computer Methods and Programs in Biomedicine 288 (2027) 109670

Contents lists available at ScienceDirect

Computer Methods and Programs in Biomedicine

journal homepage: www.sciencedirect.com/journal/computer-methods-and-programs-in-biomedicine

Human *in silico* modeling guided by transcriptomics predicts drug-induced proarrhythmicity as a function of age

Elisa Garrido-Huéscar [a,*], Ricardo Maximiliano Rosales [a], María Pérez-Zabalza [a,b,c], Pablo Laguna [a,b], Laura Ordovás [a,b,d,1], Esther Pueyo [a,b,*,1]

[a] Aragón Institute of Engineering Research (I3A), University of Zaragoza & Instituto de Investigación Sanitaria de Aragón (IIS Aragón), BSICoS group, Zaragoza, Aragón, Spain
[b] CIBER-BBN, ISCIII, BSICoS group, Madrid, Spain
[c] Defense University Centre (CUD), Zaragoza, Spain
[d] Fundación Agencia Aragonesa para la Investigación y el Desarrollo (ARAID), Zaragoza, Spain

ARTICLE INFO

Keywords:
Cardiotoxicity
Computational modeling
Transcriptomics
Aging
Drug safety
Electrophysiology

ABSTRACT

Background and objective: Unexpected cardiotoxicity is a major cause of drug failure during development and can also contribute to market withdrawal. Traditional preclinical models and clinical trials do not fully capture age-related cardiac functional decline, which is associated with increased arrhythmic risk. We aimed to develop human-based *in silico* electrophysiology models incorporating age-related remodeling to improve the assessment of age-dependent drug-induced cardiotoxicity during drug development.

Methods: Biological and chronological transcriptomic age-related human ventricular ionic remodeling was integrated into the O'Hara-Virag-Varro-Rudy model of ventricular electrophysiology at both cellular and tissue levels. Cardiac biological age was represented using two independent gene expression-based indices: SenesAge, based on one gene related to cell senescence, and AppAge, based on nearly 2,000 age-related genes. A panel of 12 reference drugs was used to evaluate age-related drug-induced cardiotoxicity.

Results: *In silico* aging based on SenesAge and AppAge reproduced age-related electrophysiological phenotypes at the cellular, tissue, and ECG levels more closely than chronological age-based remodeling. Biological age-related remodeling also increased the susceptibility to arrhythmogenic events following drug exposure by more than fivefold with respect to the adult population across the majority of tested conditions, although the effects varied according to the drug and its concentration.

Conclusions: This study provides a novel perspective for incorporating biological age-related remodeling into an established human-based *in silico* framework for preclinical cardiotoxicity evaluation at the population level. Our findings support biological age-based modeling as a complement to chronological age-based approaches for improving age-specific drug-induced cardiac risk assessment.

1. Introduction

Unexpected cardiotoxicity remains an important cause of attrition during drug development and can also lead to regulatory restrictions or withdrawal after marketing [1–4]. For cardiac safety, it is therefore important to identify proarrhythmic liabilities early in development to guide compound selection and dose assessment. Traditional preclinical strategies have relied on *in vitro* inhibition of the human ether-a-go-go related gene (hERG), which encodes the rapid delayed rectifier potassium channel [5], together with *in vivo* assessment of QT/QTc interval prolongation in animal electrocardiograms (ECGs) [6,7]. Although these approaches provide valuable information, hERG-focused assays do not account for the combined effects of multiple ion channels, and animal models do not always reproduce human-specific cardiac electrophysiology because of interspecies differences in ion-channel expression, action potential (AP) morphology, anatomy and physiology [8]. These limitations have motivated the development of human-based approaches for mechanistic and population-aware

* Corresponding authors.
E-mail addresses: elisagarrido18@unizar.es (E. Garrido-Huéscar), epueyo@unizar.es (E. Pueyo).
[1] Equal contribution

https://doi.org/10.1016/j.cmpb.2026.109670
Received 3 July 2025; Received in revised form 31 August 2026; Accepted 29 September 2026
Available online 29 September 2026
0169-2607/© 2026 The Authors. Published by Elsevier B.V. This is an open access article under the CC BY-NC license (http://creativecommons.org/licenses/by-nc/4.0/).

assessment of drug-induced cardiac risk.

In the last decade, initiatives such as the Comprehensive *In Vitro* Proarrhythmia Assay (CiPA) have promoted the use of human-based approaches, including *in silico* models, to improve the assessment of drug-induced proarrhythmic risk [9]. Population-based human ventricular models have subsequently been used to characterize interindividual variability and predict drug-induced electrophysiological abnormalities, providing mechanistic information beyond APD prolongation alone [10,11]. Nevertheless, most computational approaches have focused on adult populations and have not explicitly incorporated age-related remodeling of cardiac electrophysiology.

Age is an important but frequently neglected factor in drug cardiotoxicity assessment. Prescription drug use increases substantially with age, with particularly high use among individuals over 65 years, and the proportion of older adults in the global population is expected to increase substantially in the coming decades [12,13]. Older individuals may also be more susceptible to drug-induced electrophysiological abnormalities, including QT prolongation and ventricular arrhythmias [14–16]. However, age-related safety evaluations and computational drug-safety approaches do not routinely account for the electrophysiological remodeling associated with aging [17,18].

Aging is a complex process associated with progressive molecular, cellular and functional changes that affect cardiac function [19,20]. In the heart, age-related alterations in calcium handling, mitochondrial function, reactive oxygen species production, and extracellular matrix remodeling can contribute to increased arrhythmic susceptibility [21–23]. One clinically relevant manifestation is prolongation of the QT interval in older individuals, reflecting longer ventricular depolarization and repolarization and an increased risk of arrhythmia [24]. Older individuals also exhibit reduced tolerance to elevated heart rates, which may further influence their susceptibility to electrophysiological disturbances [25].

Despite the evidence that aging modifies cardiac electrophysiology and arrhythmic susceptibility, *in silico* models specifically incorporating human age-related ventricular electrophysiological remodeling remain limited. An *in silico* electromechanical model of age-induced remodeling was recently proposed [26], but only four model parameters were varied within fixed ranges based on animal data. An *in vitro* approach based on cardiomyocytes derived from human induced pluripotent stem cells from patients with Hutchinson–Gilford Progeria Syndrome has also been proposed [27]. However, accelerated aging associated with this pathology may not accurately reproduce the molecular and electrophysiological changes of natural aging.

In this study, we address this gap by generating human ventricular *in silico* models incorporating age-related ionic remodeling derived from experimental human transcriptomic data. These models were used to assess the effects of chronological age (CA) and biological age (BA) on cardiac electrophysiology and on susceptibility to drug-induced arrhythmogenic events. Following previous work from our group [28], two BA measures were considered: SenesAge, based on the expression of the senescence-associated gene *CDKN2A*, and AppAge, a composite biological-age measure derived from nearly 2,000 age-related genes. We evaluated the resulting adult and aged populations under different pacing conditions and following exposure to reference drugs with different proarrhythmic risk profiles. This approach provides a human-based framework to investigate how age-related electrophysiological remodeling may modify drug-induced cardiac risk and highlights the potential value of incorporating biological age into preclinical drug-safety assessment.

2. Methods

2.1. Bioinformatics analysis of age-related ionic remodeling

Left ventricle RNA-seq data of 132 male donors whose cause of death was unrelated to cardiovascular diseases were filtered from the datasets of the GTEx Portal (dbGaP accession number phs000424.v8.p2 on 06/15/2017) as previously described [28]. The study population was divided into fifths (P20, P40, P60, P80, P100) according to CA and to the two BA markers described previously [28], namely SenesAge and AppAge (**Supplementary Figure S1**). For CA, the differential gene expression ($\log_2$ fold change, $\log_2$FC) was calculated between the highest versus the lowest age fifths (*P100* versus *P20*) [28]. The $\log_2$FC values of each gene based on SenesAge and AppAge were obtained from previously reported data [28]. The statistical significance threshold for differentially expressed genes (DEGs) was set at a False Discovery Rate (FDR) ≤ 0.05 in all cases.

2.2. In silico populations of adult and aged electrophysiological models

The O'Hara-Virag-Varro-Rudy (ORd) [29] model of the endocardial ventricular cardiomyocyte (CM) electrophysiology was used as a basis to build populations of AP models representing a range of electrophysiological characteristics measured experimentally. The ORd model has been broadly used in *in silico* investigations targeting different electrophysiological applications, including the evaluation of drug effects [9,30].

To reproduce the interindividual variability of the adult human population, we initially generated a population of 10,000 models by varying the nominal conductances of seven ionic currents and the maximal current value of three pumps and exchangers involved in the AP of human ventricular cardiomyocytes: fast Na^+ current, I_{Na}; late Na^+ current, I_{NaL}; transient outward K^+ current, I_{to}; L-type Ca^{2+} current, I_{CaL}; rapid delayed rectifier K^+ current, I_{Kr}; slow delayed rectifier K^+ current, I_{Ks}; inward rectifier K^+ current, I_{K1}; Na^+/Ca^{2+} exchanger, I_{NaCa}; Na^+/K^+ pump, I_{NaK}; and sarcolemmal Ca^{2+} pump, I_{pCa}. The conductances/maximal current values were sampled in the range from 0.5 to 2 times their default value in the ORd model using the Latin Hypercube Sampling method [31]. Next, we calibrated the generated population to retain only those AP models whose electrophysiological properties lied within physiological limits, as in previous works [32]. The measured electrophysiological properties at steady state, after pacing the CMs for 1,000 beats at a basic cycle length (CL) of 1 s, were: APD_{90}, APD_{50} and APD_{40}, denoting AP duration (APD) at 90%, 50% and 40% repolarization, respectively; RMP, standing for resting membrane potential; V_{max}, measuring peak membrane potential; and AP triangulation (Tri_{90-40}) measured as the difference between APD_{90} and APD_{40}. The experimental ranges of these properties were taken from previous publications [10]. The calibrated population was defined as the basal adult population. The scaling factors applied to each calibrated model can be found in **Supplementary Table S1**.

Next, we generated populations of aged models by CA, SenesAge, and AppAge. An aged model was built from each adult model by applying scaling factors to ionic currents and fluxes, with such scaling factors being the fold change expression values (calculated from the $\log_2$FC) of the genes encoding the corresponding proteins (ion channels, pumps, exchangers, and receptors). The DEGs by BA were identified and the corresponding scaling factors by CA, SenesAge, and AppAge were applied to build each of the populations of aged models.

In the case of genes encoding channels, pumps and exchangers, the age-related scaling factor was applied to the corresponding current conductance/maximal value. In the case of genes involved in calcium handling [33], the age-related scaling factors were applied to the calcium uptake via the SERCA2a pump, J_{up}, and the sarcoplasmic reticulum calcium release flux via ryanodine receptors (RYRs), J_{rel}. Two genes involved in J_{up} were considered: *SERCA2a*, which encodes the Ca^{2+} pump SERCA2a, for which the scaling factor was applied to the total J_{up} current; and *PLN*, which encodes phospholamban (PLN), a protein that inhibits SERCA2a, thereby reducing the Ca^{2+} uptake into the sarcoplasmic reticulum [34], for which the scaling factor was applied to the half-saturation concentration of PLN ($\Delta K_{m,PLN}$). To modify J_{rel} according to the aged state, the changes observed in the expression of the *RYR*

gene, which encodes ryanodine channels, were applied as a scaling factor to the total J_{rel} current.

Simulated cells from adult and aged models were paced at CLs of 1 and 0.7 s, to mimic rest and exercise conditions, respectively, for 1,100 beats to ensure that steady state was reached. The simulations were executed in Matlab (MathWorks Inc, Natwick, MA, USA) using the ODE15s solver [35]. The last 100 beats of each simulation were analyzed to extract the values of APD_{90}, APD_{40}, Tri_{90-40}, RMP and V_{max}. Additionally, properties of the calcium transient (CaT) were extracted, including its duration at 90% and 40% ($CaTD_{90}$ and $CaTD_{40}$, respectively), its shape, represented by the CaT triangulation (CaT Tri_{90-40}), and the maximal value of free cytoplasmic Ca^{2+} (CaT_{max}). As a note, after 1,000 beats, simulations reached a steady-state behavior. The last 100 beats were then analyzed to identify arrhythmogenic events, because in models exhibiting such events, these were not necessarily present on every beat but could occur intermittently. When no arrhythmogenic event was detected, electrophysiological biomarkers were calculated over the 100 recorded beats to provide a consistent assessment of the model response.

To further validate our approach, simulations were conducted using a second basal adult model based on the ORd model with updates on several ionic currents, as published in the study by Llopis-Lorente et al. [11]. For evaluations with this second model, an initial population of 2,000 models was generated.

2.3. Simulation and assessment of drug effects on ventricular cell electrophysiology

Drug effects were modeled and simulated for adult and aged populations. Twelve reference drugs from the CiPA initiative dataset [9] belonging to the three risk categories (low, medium, high) were selected and tested at different concentrations **(Supplementary Table S2)**. The effects of the drugs on the ionic currents I_{Na}, I_{NaL}, I_{to}, I_{CaL}, I_{Kr}, I_{Ks}, and I_{K1} were described as a function of the drug concentration. In particular, the value of each ionic conductance was changed to represent the action of drug concentration C by accounting for the half maximal inhibitory concentration (IC_{50}) [36] according to the following formulation (**Equation 1**):

$$g_i^D = \frac{1}{1 + CE_i} g_i^U$$

where i is the ionic current, C is the drug concentration expressed in nM, E_i is $1/IC_{50}$ expressed in nM^{-1}, g_i^D is the ionic conductance under the drug action, and g_i^U is the ionic conductance for untreated cells.

The scaling factor applied to each current for each drug and concentration can be found in **Supplementary Table S3**. Simulations were carried out under periodic pacing at CLs of 1 and 0.7 s as described above, with the initial values of the state variables of each model taken from the last beat of the corresponding untreated model.

For each drug and concentration, the occurrence of abnormalities in the APs of each model were identified and classified into three categories: early afterdepolarizations (EADs), defined as secondary depolarizations during phase two or three of the AP; non-effective beats (NEBs), if V_{max} was under 0 mV; and incomplete repolarization (IR) when the RMP value was not reached at the time the following stimuli was delivered and no EAD was present **(Supplementary Figure S2)**. The electrophysiological properties APD_{90}, APD_{40}, Tri_{90-40}, RMP, and V_{max} were not characterized from the simulations containing AP abnormalities. EAD and NEB were considered as potentially arrhythmogenic events. IR was included as an AP abnormality for our single CM analysis. When considering whole ventricles or large ventricular tissues, IR of certain areas could cause unidirectional block [37].

2.4. Mechanisms of drug-induced, age-related arrhythmogenesis

Canonical Correlation Analysis (CCA) [38] was applied to identify the ionic current conductances with the largest contribution to drug-induced arrhythmogenicity and to assess whether such contribution differed for the three analyzed age populations (adults and aged by SenesAge and AppAge).

A matrix **X** of size N x I was built, with I being the number of currents that were varied to build the populations of models and N being the number of calibrated models. The matrix **X** contained the scaling factors of each ionic current conductance/maximal current value in the untreated populations, with the element $x_{n,j}$ corresponding to the scaling factor of the i-th conductance for the n-th model. For each age population (adult, SenesAge, and AppAge), a vector **z** of length N was generated, which contained information about the absence or presence of arrhythmogenic events. Given **X** and **z**, CCA was applied to obtain the optimal values of the canonical variables $\mathbf{w}_x$ and w_z (**equation 2**):

$$\left(\mathbf{w}_x^*,\ w_z^*\right) = \arg_{\mathbf{w}_x, w_z} \max \mathrm{corr}(\mathbf{X}\mathbf{w}_x,\ \mathbf{z}w_z)$$

where corr is the linear correlation between the projected versions of **X** and **z**, i.e. $\mathbf{X}\mathbf{w}_x$ and $\mathbf{z}w_z$. The higher the absolute value of an element in $\mathbf{w}_x^*$, the larger the contribution of the corresponding ionic conductance/maximal current value to the arrhythmogenic events contained in **z** [39]. For representation, normalized absolute values of the elements in $\mathbf{w}_x^*$, in the following denoted as $\mathbf{u}_x^*$, are plotted so they are all positive and add up to one, which facilitates the interpretation.

Two different analyses were carried out separately for each of the age populations. In the first analysis, performed separately for each of the adult and BA-aged populations, the matrix **X** contained the scaling factors of each current conductance/maximal current value for each of the calibrated models and **z** contained the number of abnormal APs under the effects of all drugs and concentrations for each of the models. In the second analysis, the matrix **X** contained only the models with abnormal APs and **z** was a binary vector with values of 1 if abnormal APs (in the form of EAD, NEB, or IR) occurred only in the analyzed aged condition but not in the adult model and 0 otherwise.

2.5. Analysis of drug effects in the ECG

For a selected subset of twelve models representing different degrees of arrhythmia vulnerability in the population, computational simulations in one-dimensional transmural ventricular fibers were conducted. To select this subset, an arrhythmogenesis risk index (ARIx) was calculated for each calibrated model of the adult population. Specifically, for each model, ARIx was defined as the sum of all cases where abnormal APs (EAD, NEB or IR) were found throughout all the simulations of that model including all the aged states, drugs, and drug concentrations paced at 0.7 s. A CL of 0.7 s was selected for the tissue simulations based on the reported reduced tolerance of older individuals to elevated heart rates [25], which may help emphasize differences in electrophysiological responses between adult and BA populations.

The models were then distributed from low to high ARIx and divided into six groups. The first group consisted of non-arrhythmogenic models (ARIx = 0), and the remaining groups were defined by increasing ranges of ARIx. Two models were randomly selected from each of the groups for inclusion in the one-dimensional ventricular fiber simulations.

Transmural ventricular fibers of 1.6 cm, composed of 40% endocardial, 25% midmyocardial, and 35% epicardial cells, were modeled. The I_{Na} formulation of the ORd model was replaced with the one of the ten Tusscher-Panfilov model [40] following the comment by O'Hara and coauthors for tissue simulations (comment on article from 05 Oct 2012 [29]) and as previously applied in other works [41]. This update on the ORd model has been reported to increase the low conduction velocity (CV) associated with the unmodified ORd model in tissue simulations [42]. The propagation of the transmembrane potential in the tissue was

described by the monodomain model according to the following reaction-diffusion partial differential equation (**equation 3**):

$$\frac{\partial V(x,t)}{\partial t} = \frac{-I_{ion}(V(x,t))}{C_m} + D\,\frac{\partial^2 V(x,t)}{\partial x^2}$$

where V(x,t) is the transmembrane potential at the spatial point x and time t, $\frac{\partial V(x,t)}{\partial t}$ is the partial derivative of the transmembrane potential at the spatial point x and time t, I_{ion} is the sum of all ionic currents (dependent on V(x,t)) and the stimulus current, C_m is the cell membrane capacitance per unit area, and D is the diffusion coefficient. Zero-flux Neumann boundary conditions were imposed.

To solve the partial differential equation, the operator splitting method was used to decouple the reaction and diffusion terms. Simulations were performed using an in-house cardiac electrophysiology solver, ELECTRA (available at https://github.com/lino202/ELECTRA), implementing the finite element method and meshless methods [43]. For this study, the Finite Element Method, with a spatial resolution of 0.01 cm, was considered. The dual-adaptive explicit integration algorithm was used for numerical time integration [44]. The initialization of the tissue models was based on the values of the state variables attained after 1,000-beat simulations in single cells. The tissue was periodically paced at a CL of 0.7 s by applying a train of 120 stimuli to the endocardial end of the fiber, with a stimulus duration of 2 ms and a stimulus amplitude of 1.5 times the diastolic threshold.

Pseudo-ECGs (pECGs) were computed from the simulated transmembrane potentials by calculating the extracellular potential recorded by an electrode placed 2 cm away from the epicardial end of the fiber in the direction of the fiber axis, as in previous works [45]. Specifically, the pECG signal was calculated at each time instant t according to the following equation, with its amplitude being subsequently normalized to have a maximum amplitude value of 1 (**equation 4**):

$$\psi(x',t) = -\int_{x=0}^{x=L} \sigma\,\nabla_x V(x,t)\cdot\nabla_x\left(\frac{1}{r(x,x')}\right)dx$$

where σ is the diffusion coefficient of the surrounding electrical medium, L is the fiber length, and r(x,x') is the distance between a point within the fiber x and the electrode recording the signal at a point x' outside the fiber but in its axis direction.

The QT interval and T-peak-to-T-end (Tpe) interval were computed from the pECGs by using an in-house software [46] that includes a delineation system based on the wavelet transform to identify the onsets, peaks, and ends of the ECG waves. The QT interval was measured from the onset of the QRS complex to the end of the T wave. The Tpe interval was measured from the peak to the end of the T wave. With the fiber being paced at the endocardial end, CV was calculated as the distance covered between a cell near the endocardial end and a cell near the epicardial end divided by the difference in their corresponding activation times, which were computed from the maximum derivative of the AP upstroke.

3. Results

3.1. *In silico aging guided by transcriptomics describes age-related changes in cellular electrophysiology*

To study the effects of age on ventricular cell electrophysiology, we started by generating a representative population of electrophysiological models for adult ventricular cells. Taking the basal ORd model and varying the model parameters corresponding to several ionic current conductances and maximal current values of pump and exchanger currents, a population of 10,000 models was generated. Of these, 1024 models successfully passed the calibration with human experimental data on AP electrophysiological properties, resulting in a total of 1025 models when including the basal ORd model too (Fig. 1A). In the calibration, the electrophysiological properties that proved to restrict the most the number of calibrated models were Tri_{90-40} and V_{max}, with only 56.85% and 23.61% of the models falling within the physiological ranges for these two properties (Fig. 1B).

To feed the *in silico* models with aging features, we characterized the BA-related electrophysiological remodeling in the human left ventricle using bulk tissue transcriptomics from a previous study [28] and we calculated it for CA (Fig. 1C, **Supplementary Tables S4–5**). Differential gene expression analysis by CA showed that all the analyzed genes were downregulated in the elderly, but only genes involved in calcium release and uptake into the sarcoplasmic reticulum (*SERCA2a* and *RYR2*) and those contributing to recover the intracellular and extracellular ion concentrations from one beat to the next (*SLC8A1* and *ATP1A3* encoding the Na^+/Ca^{2+} exchanger and the Na^+/K^+ pump, respectively) showed significant downregulation. Age defined by SenesAge and AppAge emphasized these changes with respect to CA. For these two BA descriptors, all the genes presented significant changes in biologically older individuals (Fig. 1C, **Supplementary Table S4–5**), with the differences being more pronounced for AppAge.

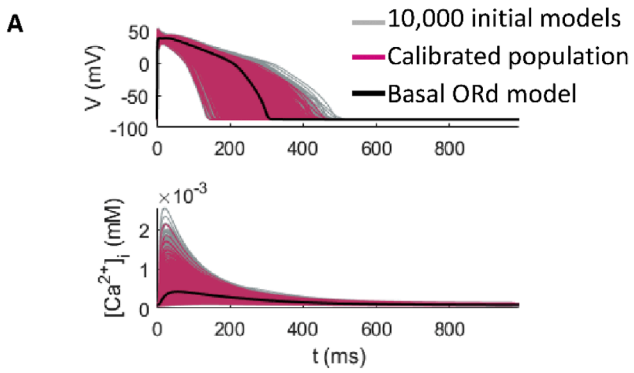
By first taking the default ORd model and its aged versions, we sought to investigate the effect of age-related ionic remodeling on the ventricular cellular electrophysiology, considering both AP and CaT properties. Applying the CA-related scaling factors for ionic current conductances, maximal current values and receptor characteristics (**Supplementary Table S4**) to the default ORd model at CL = 1 s led to minimal changes in the AP duration and shape. Instead, the AP was notably prolonged when age was considered by BA, even if the AP presented a plateau phase like that of the adult model (Fig. 1D). Under a more accelerated pacing rate (CL = 0.7 s), the AP shape and duration followed the same changes as observed for CL = 1 s. Regarding CaT, we found that CaT_{90} was prolonged by all types of age at both CLs. For CaT_{max}, the impact of age-related ionic remodeling was negligible at a CL of 1 s, while at CL = 0.7 s all age types led to a slightly higher peak (Fig. 1D).

Next, we compared the whole constructed populations of adult and aged models. An evident increase in APD was observed in both BA-based populations, but not in the CA-based population, for the two tested CLs (Fig. 1E). The morphology of the AP also changed in both BA populations, with an increase in Tri_{90-40}, while much less pronounced effects were observed with CA for the two tested CLs (Fig. 1F). Regarding CaT, its duration was prolonged in all aged populations, with more pronounced effects for BA than CA (Fig. 1G), with these observations holding for both CLs but more acutely at a CL of 1 s. Age also influenced CaT_{max} (Fig. 1H). We found that CaT_{max} was increased in the aged groups compared to the adult group, with this increase being more pronounced for BA than for CA at both CLs.

We also assessed whether BA altered the APD_{90} rate dependence. APD_{90} showed a clear CL dependence in both adult and BA populations. In the adult population, the median APD_{90} values were 260.21, 281.15, 300.01, and 311.01 ms at CLs of 0.7, 1, 1.5, and 2 s, respectively. Relative to adult, APD_{90} was prolonged by 63.38, 62.58, 64.58, and 66.54 ms in SenesAge and by 85.27, 83.11, 83.81, and 85.41 ms in AppAge at the corresponding CLs. Thus, BA remodeling resulted in a consistent upward shift in APD_{90} across the tested CLs, with a greater prolongation in AppAge than in SenesAge. However, the difference between the median APD90 at the longest tested CL (2 s) and the shortest tested CL (0.7 s) was similar across groups: 50.81 ms in adult, 53.96 ms in SenesAge, and 50.94 ms in AppAge. These results indicate that the principal effect of BA remodeling was an upward shift in APD_{90} rather than a substantial alteration in its dependence on pacing CL.

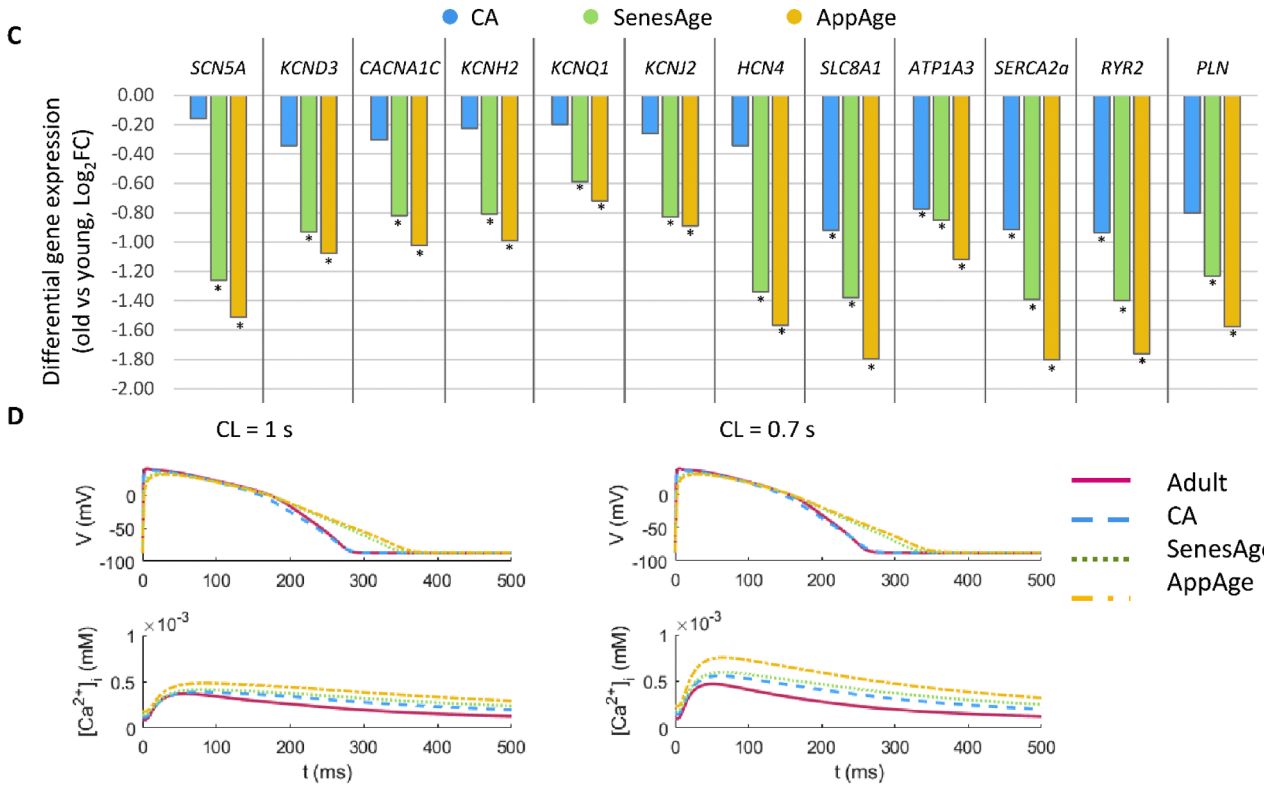
Our findings on the effects of age on human ventricular electrical activity were confirmed using a second model, i.e. the ORd-based model employed by Llopis-Lorente et al. [11], on a calibrated population of 113 models (**Supplementary Figure S3**).

Therefore, the observed changes for BA-based transcriptomic-guided



B

Calibration Parameter	Nº of models that meet each criterion
APD_{90}	8974
APD_{50}	9935
APD_{40}	9997
Tri_{90-40}	5686
RMP	10001
V_{max}	2362



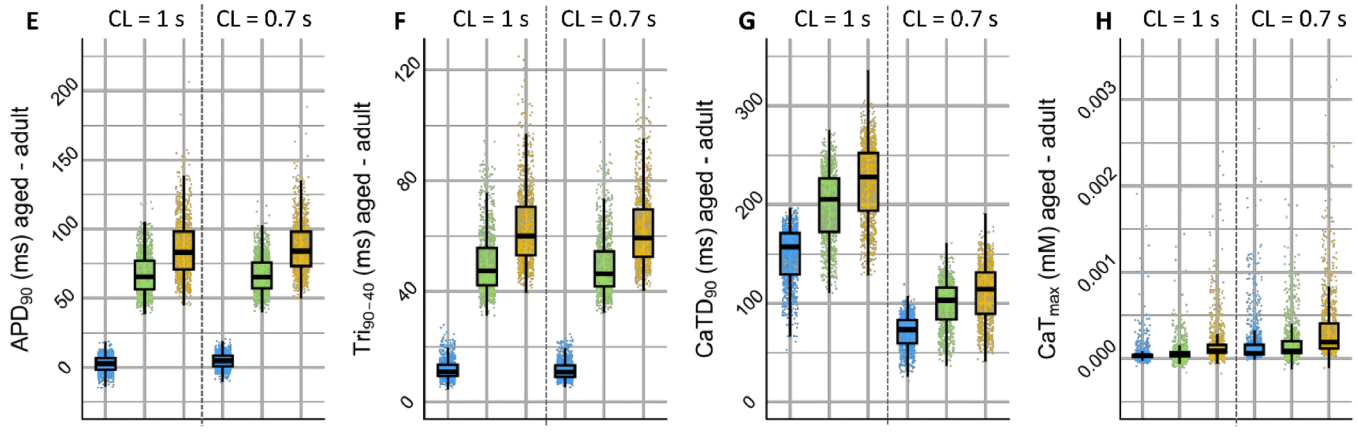


Fig. 1. Generation of adult and aged populations of models. A) Calibration of the adult population. The AP and CaT of the 10,000 generated models are represented in grey, while the 1025 models that passed the calibration process are highlighted in pink. The basal Ord model is represented in black. **B)** Number of models fulfilling each of the experimental calibration criteria. **C)** Differential gene expression in elder (P100) vs young (P20) individuals (as Log_2 fold change - Log_2FC - values) for CA and BA (SenesAge and AppAge) (*FDR < 0.1) of genes encoding for ion channels involved in the cardiac action potential included in the Ord model. **D)** Age-induced effects on the AP and CaT of the basal ORd model for the analysis using either CA or BA (SenesAge and AppAge). **E-H)** Boxplots of changes in the AP (APD_{90} -E- and Tri_{90-40} -F-) and CaT ($CaTD_{90}$ -G- and CaT_{max} -H-) for the aged populations with respect to the adult population. Each point corresponds to one model. In all figures CA, SenesAge and AppAge are color coded in blue, green and orange, respectively. Cicle length (CL) of 1 s and 0.7 s are represented for all parameters.

in silico aging qualitatively agree with experimental and review evidence from various animal aging models [47–49] and the well-documented age-related QT/QTc prolongation in humans [24,50,51], while changes quantified from CA-based *in silico* models did not adequately reproduce them. In the following, only BA populations will be considered for the *in silico* aging analysis.

3.2. The adverse cellular electrophysiological effects of drugs are more pronounced in aged populations

We investigated the effect of age in the arrhythmogenic potential of a first set of six reference drugs with different arrhythmogenic risk (from low to high) at four different concentrations **(Supplementary Table S2)**. For the lowest concentration (C1 = C_{max}), arrhythmogenic events (EAD and NEB) were only found for AppAge at CL of 0.7 s and always in a minimal number of cases (below 0.9% of the models) (Fig. 2). The median APD_{90} prolongation was in all cases up to 100 ms for this concentration. For concentrations from C2 to C4, with the latter corresponding to 25 times C_{max}, the higher the concentration and the risk category of the drug, the larger the APD_{90} prolongation and/or the increase in the percentage of models presenting arrhythmogenic events in the adult population. The median APD_{90} prolongation was in all cases higher at a CL of 1 s than at a CL of 0.7 s. The percentage of models presenting arrhythmogenic events was higher at a CL of 0.7 s except for the higher doses of the high-risk drugs (bepridil C3 and C4, dofetilide C4) (Fig. 2 **and Supplementary Figure S4**).

When comparing the aged populations with the adult one, the effects were in most cases emphasized for the BA populations. The APD_{90} prolongation (for both CL 1 s and 0.7 s) and the increase in arrhythmogenic events (for CL 0.7 s in all cases, and CL 1 s for almost all conditions) were consistently higher for the BA populations than for the adult one, with the drug effects being more marked for AppAge than for SenesAge, although the magnitude of these differences varied for different drugs. Of note, the CiPA risk categories did not translate directly into the proportion of models exhibiting arrhythmogenic events after age-related remodeling was incorporated. While the expected differences between risk categories were more apparent in the adult population, the response of the biologically aged populations was shifted toward greater susceptibility. For example, APD_{90} prolongation was comparable for medium-risk drugs in BA-aged populations (e.g. cisapride at C3) and for high-risk drugs in adult populations (e.g. dofetilide at C3). Similarly, both low-risk drugs, which posed no risk in the adult group, induced APD_{90} prolongation and a proportion of arrhythmogenic events in BA populations comparable to those of mid-risk drugs in adults, especially at CL 0.7 s (Fig. 2).

A closer examination of the AP abnormalities revealed that the AppAge population exhibited a higher proportion of NEB and IR compared to both the adult and SenesAge populations (**Supplementary Figure S4**). Conversely, EADs were the most prevalent AP abnormality in the adult population, even slightly exceeding the proportion of models presenting this abnormality in the AppAge and SenesAge groups under certain conditions, such as C3 of cisapride, bepridil, and dofetilide at CL 0.7 s, or these same drugs at C4 across both CLs. NEBs were only observed in the adult population under the highest concentration (C4) of cisapride, dofetilide and bepridil, but were observed in BA populations for all drugs (**Supplementary Figure S4**).

We additionally tested the drug effects on APD_{40} to provide information on the changes in the phase 2 of the AP, observing that drugs blocking K^+ channels (e.g., ranolazine, cisapride) led to a slightly higher prolongation of APD_{40} in the adult population than in the aged groups. In contrast, the calcium channel blocker diltiazem minimally prolonged APD_{40} in the adult population but more strongly prolonged APD_{40} in both BA groups. The drug-induced APD_{40} prolongation was slightly more pronounced at a CL of 1 s than at 0.7 s in all cases (**Supplementary Figure S5**). In concordance with the drug effects on APD_{40} and APD_{90}, we observed that all drugs except for diltiazem led to more triangular APs, with this effect being more pronounced in the aged than the adult populations and at a CL of 1 s than at 0.7 s (**Supplementary Figure S6**).

The drug effects on RMP were negligible, with the largest magnitude of change being below 2 mV and the median increments being below 0.5 mV for all drug concentrations and CLs (**Supplementary Figure S7**). For V_{max}, only diltiazem at concentrations C2-C4 led to a noticeable reduction in this marker at the two CLs, with such a reduction being more marked for the BA populations than for the adult population (**Supplementary Figure S8**) and leading to the appearance of NEB in the aged populations (**Supplementary Figure S4**).

In the case of the CaT amplitude, duration and shape, drug effects had a larger impact on the adult population than on the BA ones, with those effects being more pronounced for the calcium channel blocker diltiazem. CaT duration was more affected at a CL of 1 s, while its shape and amplitude suffered a larger drug-related effect at a CL of 0.7 s (**Supplementary Figures S9– 11**).

The effects of the six reference drugs in the second set **(Supplementary Table S2)** were also notably more pronounced on the BA populations compared to the adult one **(Supplementary Figures S12– 13)**, supporting the conclusions obtained for the first set of tested drugs.

To further investigate the effect of pacing rate on the age-related susceptibility to electrophysiological abnormalities under drugs, simulations were performed at two additional slower pacing rates (CL = 1.5 s and CL = 2 s) using a medium risk drug, ranolazine, at concentration C4 (**Supplementary Figure S14**). As expected, the number of EADs was higher whereas the numbers of IR and NEB were lower than those observed at higher pacing rates. Importantly, the proportion of models exhibiting abnormal APs remained higher in the AppAge population than in the adult population at both cycle lengths. For the SenesAge population, a higher proportion of abnormal APs than in the adult population was observed at CL = 1.5 s, whereas at CL = 2 s the proportion was similar to that observed in the adult population (**Supplementary Figure S14**).

Hence, the response to drugs in the biologically aged populations was notably different than in the adult one, supporting the interest of preclinically studying age-related drug cardiotoxicity in aged individuals.

3.3. CCA analysis reveals the major contributors to drug-induced electrophysiological abnormalities as a function of age

To understand the electrophysiological basis of the drug-induced adverse effects in the adult and aged populations at the pacing condition (CL 0.7 s) at which the largest age-related differences in drug-induced arrhythmogenic events were observed, CCA was applied individually in each population (Fig. 3A). Diltiazem was analyzed separately from all the other drugs due to the different mechanism of action of this specific calcium blocker (Fig. 3B). In the first analysis aimed at ascertaining the contribution of each ionic conductance/maximal current value to the generation of AP abnormalities in each age population, our results identified differences in the relative ionic contributions in the BA and adult populations (Fig. 3A–B). In the BA populations, reductions in g_{Na}, g_{Kr}, g_{Ks}, g_{K1} and g_{NaK}, together with an increase in g_{Ca}, were among the ionic changes associated with the occurrence of abnormal APs. In the adult population, g_{Kr} and g_{Ks} showed the strongest contributions, while g_{Na}, g_{K1} and g_{NaK} also contributed to the separation between models with and without AP abnormalities, although to a lesser extent. The values of the correlation coefficient in the CCA analysis were particularly strong in the BA populations: adult, 0.6813; SenesAge, 0.9509; and AppAge, 0.9338.

The implication of different currents in the generation of AP abnormalities in the BA population compared to the adult one can be explained by the distinct types of AP abnormalities found in those populations. A decrease in g_{Na} was tightly related to the appearance of NEB, as the sodium current is involved in the phase 0 (depolarization) of

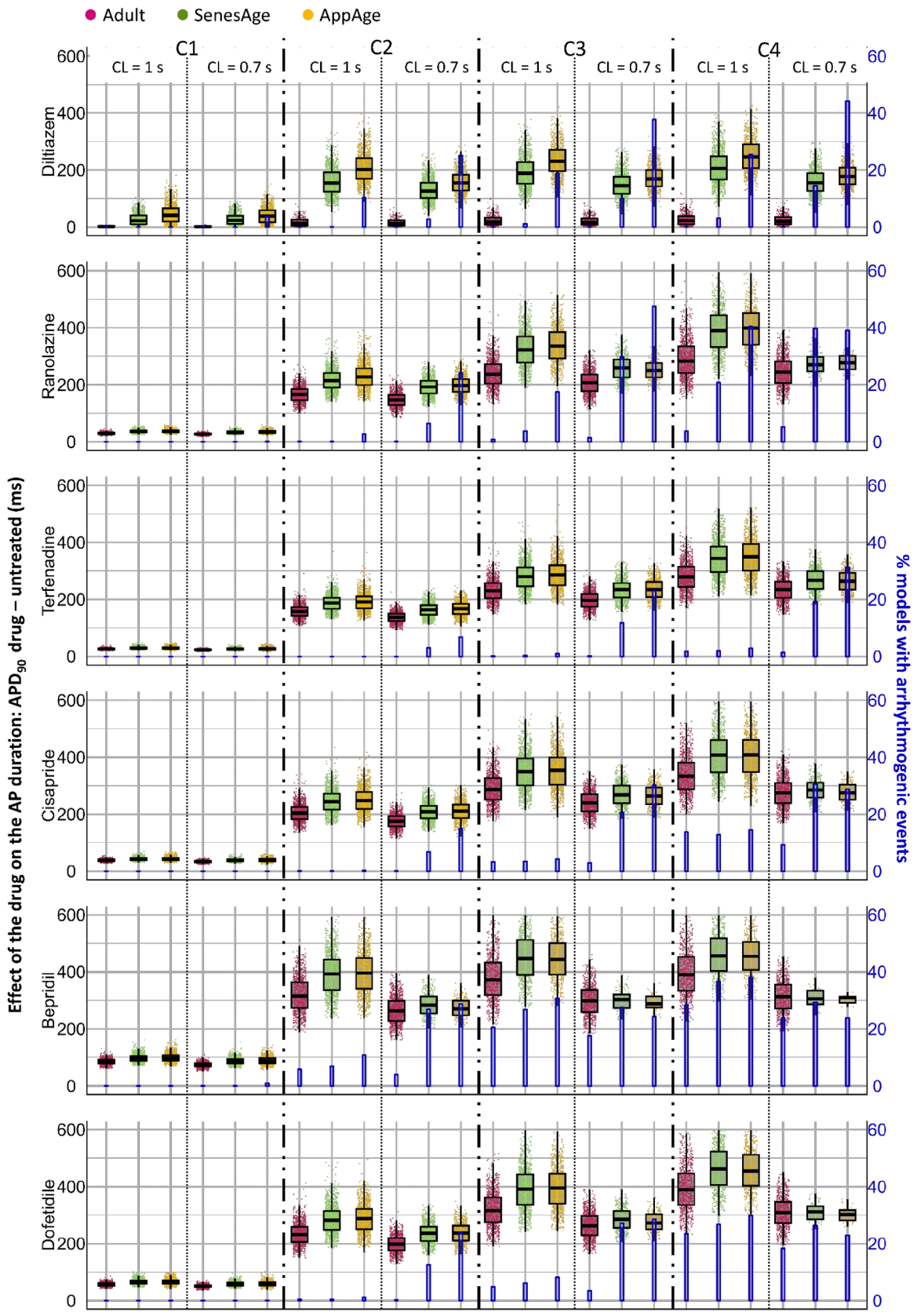


Fig. 2. Evaluation of drug effect at the endocardial cell level. Boxplots show in the left axis the difference in APD_{90} before and after treatment with set 1 drugs (diltiazem, ranolazine, terfenadine, cisapride, bepridil, dofetidile) at four different concentrations (C1=C_{max} to C4=25xC_{max}) in adult (pink) and BA-aged populations (SenesAge – green – and AppAge -yellow-). Blue bars represent in the right axis the percentage of models showing arrhythmogenic events (early afterdepolarization -EAD- and non-effective beats -NEB-) under each tested condition (right axis).

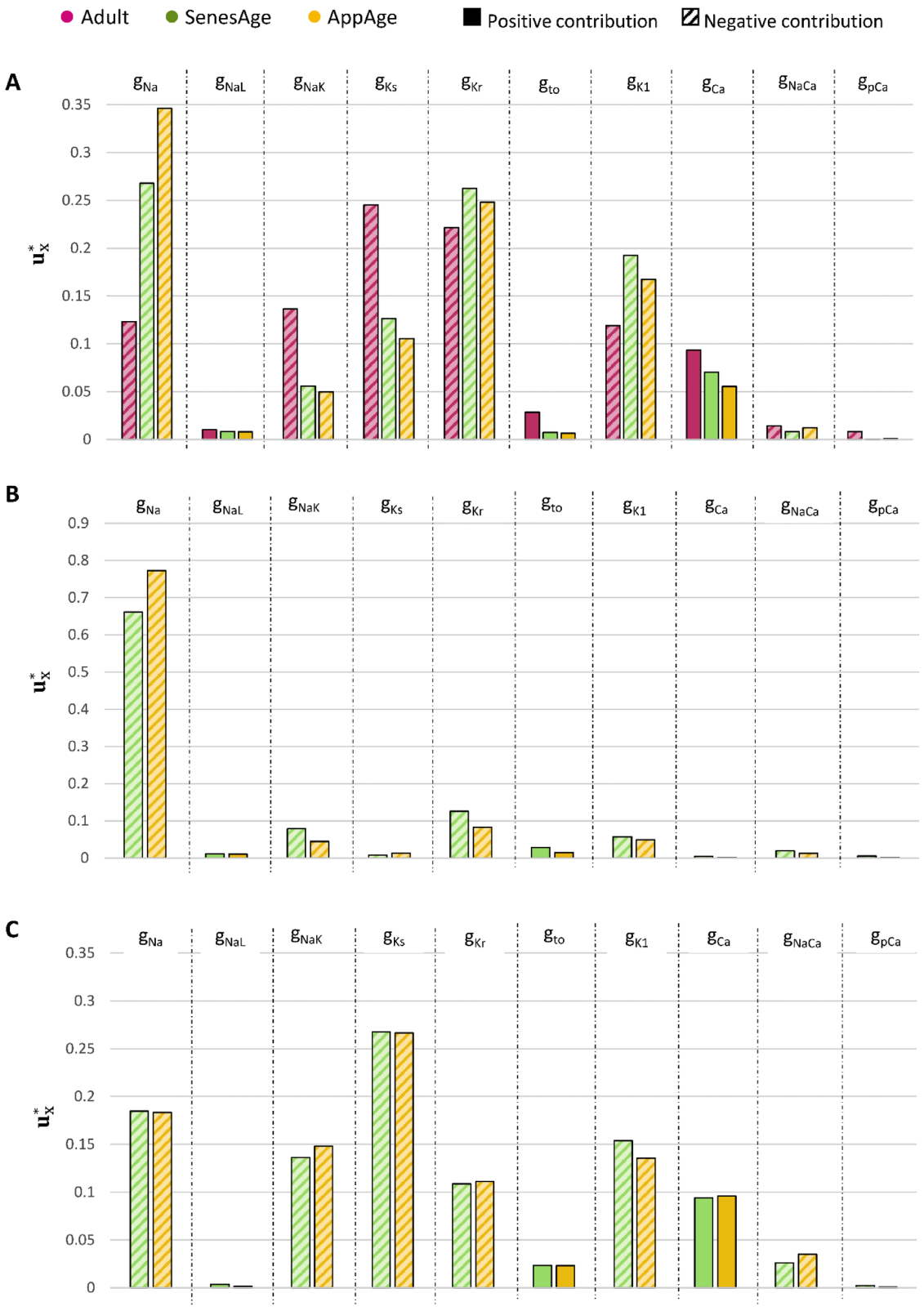


Fig. 3. Analysis of major AP-contributors to drug-induced abnormalities in adult and aged populations by canonical correlation analysis. A) Contribution of each ionic conductance / maximal current value to AP abnormalities under all drugs but diltiazem. B) Contribution of each ionic conductance / maximal current value to AP abnormalities under diltiazem. C) Contribution of each ionic conductance / maximal current value to a differential arrhythmogenic behavior between old and young. In all panels, solid bars indicate a positive contribution (the higher the parameter value, the larger its contribution to arrhythmogenicity), while striped bars indicate a negative contribution (the lower the parameter value, the larger its contribution to arrhythmogenicity). The sign of the contribution, represented by the striped and solid bars' patterns, were determined according to the signs of w_x^* and w_z^*.

the AP. The involvement of this current was stronger for the BA populations than for the adult population, as g_{Na} was reduced by more than half in both SenesAge and AppAge populations with respect to the adult one (**Supplementary Table 4, Supplementary Figure S15**). A reduction in the outward I_{Ks} and I_{Kr} currents involved in the AP plateau and repolarization, with current conductances g_{Ks} and g_{Kr}, showed to be related to IR and EAD occurrence, while a reduction in g_{K1} seemed to be important for the generation of all types of AP abnormalities (IR, EAD and NEB) (**Supplementary Figure S15**).

EAD was the most common type of AP abnormality in the adult population, followed by IR, which explains the importance of g_{Ks} in this group in comparison with both BA populations, in which IR and NEB gained more relevance (**Supplementary Figure S4, Supplementary Figure S13)**. In the two BA populations, the age-related scaling factors resulted in reductions in the outward currents $I_{Ks,}$ I_{Kr}, and I_{K1} of approximately 40%, which could explain their relevance in the occurrence of AP abnormalities when drugs that block them were added (**Supplementary Table 4**). These changes reduced the repolarizing capacity and, together with changes in other inward currents, could contribute to the increased susceptibility to prolonged APs and electrical instabilities observed in the BA population (Fig. 3A). A higher value of g_{Ca} was uniquely related to EAD (**Supplementary Figure S15**). Also, a lower value of the maximal NaK current, g_{NaK}, showed to be related to the occurrence of drug-induced EAD and NEB. g_{NaK} played a more significant role in the risk of AP abnormalities in the adult population compared to the BA populations, likely due to its involvement in the development of EADs, which are proportionally more prevalent in this group. Although g_{Ca} was also reduced in both BA populations, its contribution to the risk of AP abnormalities under drug treatment remained consistent across all groups (**Supplementary Figure S15**).

As for diltiazem, the analysis was not conducted for the adult group, as no model showed abnormal APs for any concentration of the drug (Fig. 3B). In the BA populations, a strong negative relationship was observed between g_{Na} and the occurrence of NEBs (Fig. 3B), which was the only type of AP abnormality observed under this drug (**Supplementary Figure S4**). The scaling factor of each model for g_{Na} and all other ionic currents or pumps under the effect of diltiazem are presented in **Supplementary Figure S15** for the different type of abnormalities, particularly NEBs. Nevertheless, the value of the correlation coefficient was lower than in the case of the analysis of all the other drugs together: 0.8105 for AppAge and 0.5751 for SenesAge.

Next, we performed a second analysis aimed at uncovering the ionic conductance/maximal current values that most strongly contribute to the differential risk for arrhythmogenic events in the aged state versus the adult state (Fig. 3C). For each BA-aged population, only those models exhibiting AP abnormalities under the effect of any drug (except for diltiazem) at any concentration were selected, which were 964 and 797 out of the total 1025 models for SenesAge and AppAge, respectively. The values of the correlation coefficient were high: 0.7381 for SenesAge and 0.7321 for AppAge. CCA showed that a reduction in g_{Ks}, g_{Na}, g_{NaK}, and g_{K1} were the major contributors to the largest differences in drug-induced AP abnormalities in old vs adult models. These results are in concordance with the fact that most models presenting AP abnormalities under the effects of drugs in the BA-aged population but not in the adult one showed IR or NEB, while the proportion of EADs was similar in both groups. IRs were mainly related to a reduction in the repolarization currents and NEBs to a reduction in the I_{Na} current, all of them strongly reduced in the BA populations.

3.4. Simulations at the tissue level confirm aging as a risk factor for drug-induced arrhythmia susceptibility

Next, we simulated the electrical activity in one-dimensional ventricular fibers at a CL of 0.7 s because the largest differences in drug-induced arrhythmogenic events between adult and BA populations were observed at this CL. To select a subset of models representative of all the arrhythmogenic susceptibilities within the population, we calculated the ARIx of each adult model (Fig. 4A). ARIx values ranged from 0 to 65 across all models in the study. A small fraction (0.78%) had an ARIx of 0 (group 1), while 28.20% fell within the 1–13 range (group 2). Group 3 (ARIx 14–25) contained the largest proportion, comprising 36.98% of the population. Additionally, 26.05% of models had ARIx values between 26–38 (group 4), whereas only 6.34% and 1.66% fell within the 39–50 (group 5) and 51–65 (group 6) ranges, respectively. We took two models from each of the six ARIx groups, including the default ORd model (ARIx = 17).

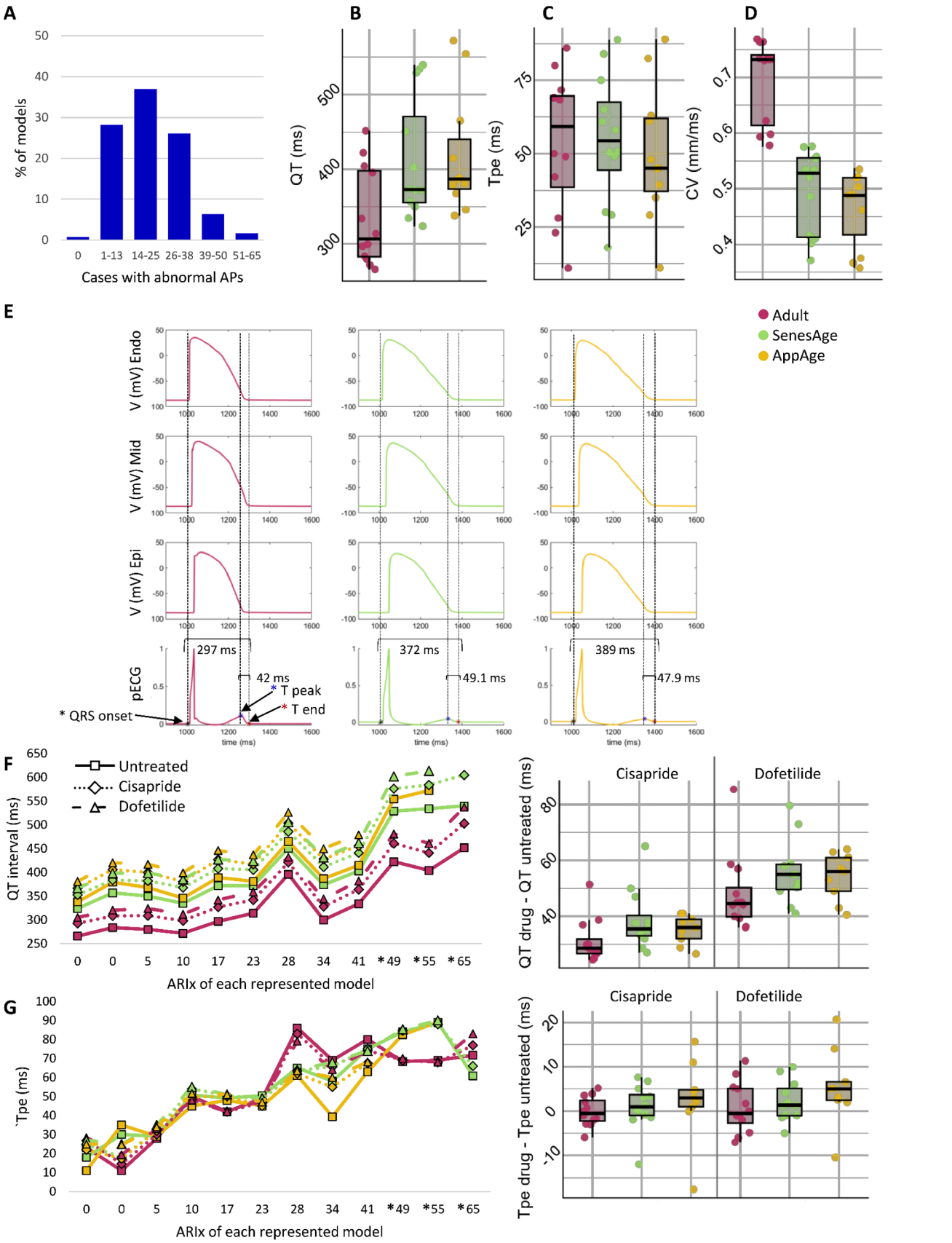
Evaluation of the QT and Tpe intervals of the pECGs calculated for the twelve selected models showed that the QT interval was prolonged in the BA populations with respect to the adult population, while the Tpe interval did not change notably. The IQR was larger in the two BA groups, which was indicative of higher inter-individual variability with age (Fig. 4**B-C, E**). Moreover, CV in the BA populations decreased compared to the adult one (Fig. 4**D**).

To characterize the potentially differential effects of drugs at the tissue level in the adult and aged groups, we tested the lowest concentration (C1, corresponding to C_{max}) of the medium-risk drug cisapride [52], as it showed similar effects in the cellular AP of BA myocytes to high-risk drugs in the cellular AP of adult myocytes (Fig. 2). We also included the high-risk drug dofetilide at the lowest concentration (C1) to assess its effects at the tissue level. For both drugs, the two and the three models with the highest ARIx (>46) when aging was induced by SenesAge and AppAge, respectively, presented NEBs, with only one every two stimuli generating an AP. For models that did not show AP abnormalities, the QT interval was found to exhibit an overall rising trend with increasing ARIx, with the QT values being higher for the BA populations than for the adult one (Fig. 4F**, left panel**). Also, the tested drugs prolonged the QT interval to a larger extent in the BA models than in the adult ones (Fig. 4F**, right panel**). The Tpe interval did not follow a clear trend in relation to the ARIx value, but, for most models, the Tpe value was higher for the BA populations than for the adult one (Fig. 4G**, left panel**). The drug effects on the Tpe interval were minimal, with a median increase of <5 ms in all age groups under both tested drugs (Fig. 4G**, right panel**). Since these two drugs primarily block I_{Kr} channels, no changes were observed on CV (data not shown).

4. Discussion

Age has been reported to prolong the AP of ventricular myocytes and consequently increase the values of the QT/QTc interval of the ECG [24]. This age-related electrophysiological remodeling may increase susceptibility to drug-induced arrhythmogenesis, particularly under drugs with potassium channel block effects. Nevertheless, older individuals remain underrepresented in many drug-development studies, despite their high medication use and increased susceptibility to age-related cardiovascular complications. The development of human-based tools that allow preclinical assessment of drugs in an age-related manner at a population level could thus constitute an important advance in the prevention of cardiotoxic effects in the elderly.

Here, we introduce the development of in silico cell and tissue electrophysiological models that describe the human ventricular ionic remodeling occurring with age at the transcriptomic level. While gene expression at the mRNA level is not strictly explaining protein function, the approximation between changes (induced by age or any other condition) in mRNA expression levels and in the conductances of the ion channels, pumps and exchangers they encode has already been employed in previous studies modeling AP differences between myocyte populations (e.g. failing versus non-failing myocytes) [53]. Obtaining equivalent information at the proteomic level, in terms of robustness (132 individuals used in this study) and with sufficient sensitivity to detect low represented proteins within the heart proteome, such as ion channels, remains highly challenging, as these are poorly isolated from the plasma membrane and represent a low proportion of the total



(caption on next page)

Fig. 4. Arrhythmogenesis risk index (ARIx) distribution and pseudo-ECG-derived indices. A) Histogram of models according to its arrhythmogenic index ARIx categorized in six groups. **B-D)** Boxplots of QT interval, Tpe interval and CV, respectively, for a subset of models representative of each ARIx category for all the studied age types. **E)** APs for the default ORd model and the corresponding age models by SenesAge and AppAge corresponding to an endocardial node (Endo) at one end of the fiber, a midmyocardial node (Mid) in the middle of the fiber and an epicardial node (Epi) at the other end of the fiber, shown together with their corresponding pseudo-ECGs. **F)** QT interval for models ordered from low to high ARIx (left panel) and boxplots of drug-induced QT interval prolongation (right panel). **G)** Analogous results for Tpe. * indicates models with drug-induced abnormal APs for SenesAge and/or AppAge, which were not included in the calculations. The duplicated 0 in the x axis corresponds to two models in group 1, i.e., models that did not exhibit any arrhythmogenic event under any of the tested drug conditions and concentrations. The age types are color-coded in all the figure as adult in pink, SenesAge in green and AppAge in yellow.

protein content compared to other protein families like sarcomeric proteins. Therefore, in this study, we approximate the changes measured at mRNA level as proportional changes in protein and electrophysiological function via the ionic current conductance/maximal current value to incorporate them into computational models of age-related human ventricular electrophysiology (**Supplementary Table S4**).

Aging is well known to happen at different rates in individuals of a population [54]. Thus, studying aging chronologically is limited by the high interindividual variability associated with the different aging rates. BA instead accounts for both the aging rate (genetics and environment) and CA of individuals. Our group reported two human cardiac BA biomarkers based on gene expression [28] and here we show that, despite their distinct complexity and, therefore, biological meaning, both yield qualitatively similar functional results across simulations. Remarkably, CA-based *in silico* aging is unable to reproduce electrophysiological aging phenotypes observed in animal models and human ECG data. In combination, the data supports the reliability of BA over CA when assessing age-related electrophysiological changes and confirms the higher sensitivity of BA to detect significant functional changes between adult and older populations (Fig. 1 **D-H, Supplementary Figure S3 C-G**). In particular, by introducing the BA-induced ventricular remodeling into *in silico* AP models, we show that BA leads to a prolongation of the APD at cell and tissue levels and of the QT interval of the ECG, in agreement with a variety of studies reporting a prolongation of ventricular repolarization with age [24,26,49,55]. The transcriptomic changes occurring with CA in the human heart are insufficient to capture this well-established phenotype *in silico*, as the number of DEGs in older individuals compared to young individuals is low and not all the genes found to be differentially expressed with CA play a major role in the APD.

Additionally, we show in the present study that CaT is altered with age (Fig. 1**G and H**), with its duration being highly prolonged, especially in BA-old compared to CA-old individuals (Fig. 1**G**), which is in agreement with published experimental works that report an impairment in the calcium handling with age, even if the causes for such dysfunction are poorly studied in humans [56]. A study using human atrial trabeculae of adult and older individuals showed a reduction in SERCA2a and PLN with age [57], which is in line with the age-modulated CaT properties introduced in our *in silico* models. A slowed sarcoplasmic reticulum Ca^{2+} sequestration and a prolongation of the CaT with age was reported in another study [58]. Using our *in silico* model, we show that the age-induced remodeling in calcium handling proteins is indeed reflected as a prolongation of the CaT. Although additional studies have shown changes in the calcium/calmodulin dependent protein kinase II gamma (*CAMK2G*), a protein involved in the regulation of both SERCA2a and ryanodine receptors [59], the gene expression was found not to be significantly different between younger and older individuals either by CA or by BA in our transcriptomic data.

Regarding the effects of drugs with age (**Supplementary Table S3)**, we observe that, in addition to the already prolonged APD in BA populations, drugs with a blocking effect of potassium channels increase cellular APD more markedly in the BA-old populations than in adults. In general, the effect of the various tested drugs is more accentuated in BA populations compared to adults. For instance, the calcium channel blocker diltiazem prolonged APD_{40} and reduced V_{max} to a greater extent in BA populations than in adults. Similarly, drugs that block potassium channels have a more significant impact on APD_{90}, Tri_{90-40} and CaT amplitude in BA populations. This may relate to the pharmacodynamics effects of the drugs according to which, for the same concentration of a ligand, a reduction in the receptor availability can lead to an increased effect of the ligand, since the proportion of free receptors decreases [60]. These findings indicate that drug-risk classification cannot be considered independently of the electrophysiological background of the population being evaluated. Although the CiPA categories provide an important framework for characterizing drug-induced proarrhythmic risk, age-related remodeling may alter the susceptibility of cardiac tissue to the same pharmacological perturbation. Consequently, compounds classified as low or medium risk in reference populations may produce more pronounced electrophysiological effects in biologically aged populations (Fig. 2**, Supplementary Figures S4– 14**).

To confirm whether the observed differences in the effects of drugs with age vary depending on the pacing rate, we investigate the response to both a pacing CL corresponding to resting conditions and to a pacing CL corresponding to elevated heart rates as those found during light or moderate exercise. In untreated populations, the AP properties exhibit minimal variation between the two tested CLs, which is in line with published studies that recommend moderate exercise for the elderly, highlighting its protective role [61]. However, under drug treatment, the increase in the pacing rate results in a marked increase in arrhythmogenic events, which agrees with studies reporting a reduced tolerance of the elderly to elevated heart rates [25]. These results suggest that the increase in heart rate due to exercise is not necessarily associated with increased risk in the elderly, but in older individuals receiving medication, closer monitoring might be needed.

The greater differences observed between adult and BA populations at a CL of 0.7 s should be interpreted in the context of the specific electrophysiological remodeling represented in our models and should not be generalized to all pacing conditions. Slower pacing rates can also promote repolarization abnormalities such as EADs, and our additional simulations at CL = 1.5 s and 2 s confirm that age-related differences in susceptibility can persist at slower rates, although their magnitude depends on the BA definition and pacing rate (**Supplementary Figure S14**).

By CCA, our study uncovers the conductances of ionic currents and maximal current values of pumps and exchangers that lead to the largest differences in drug-induced AP abnormalities between elder and adult populations at 0.7 s pacing rate. These include reductions in the conductances of I_{Na}, I_{Ks}, and I_{K1} and in the maximal current value of I_{NaK}, which lead to a large increase in the number of models showing IR or NEB in the BA populations, while the proportion of EADs remains similar in both adult and elderly (Fig. 3**, Supplementary Figure S15**).

Due to the challenges in accessing live healthy human cardiac tissue and the limited availability of information on cardiac electrophysiology at the cellular level, especially regarding a comparison between adult and older individuals, tissue simulations were conducted and pECGs were calculated to establish a comparison with experimental and clinical studies. In our populations of models, the mean QT interval at a pacing CL of 0.7 s was prolonged by 73.69 ms and 90.70 ms in older models by SenesAge and AppAge, respectively, compared with the adult population (Fig. 4B). Clinical studies have reported a mean QTc prolongation in older versus younger adults of approximately 30 ms [24,51]. The larger QT prolongation observed in our study for both BA groups compared to the commonly reported QT interval prolongation in old subjects may result from several factors, including the limited availability of studies

investigating QTc prolongation according to BA rather than CA, the simplicity of the tissue simulations performed in one-dimensional tissue fibers rather than two-dimensional tissue sheets or three-dimensional volumes, and the fact that the aging factors were derived from RNA expression rather than protein measurements. In addition, tissue simulations were conducted for twelve models, which, although they recapitulate a broad spectrum of basal arrhythmic risk, overrepresent the subpopulation at higher arrhythmic risk and may therefore exhibit longer repolarization durations. It should be noted that structural age-related remodeling, such as fibrosis [62], was not explicitly incorporated into the present electrophysiological model. However, the molecular data used to simulate the ionic remodeling originates from human tissue, where the effects of aging at the structural, whole organ and even organism levels are represented. Consequently, even if the simulated effects should be interpreted primarily as the consequences of age-related molecular remodeling represented by the selected transcriptomic factors and more complex models could be developed including structural remodeling, it is worth nothing that these factors represent the global effect of aging in the human heart. Despite these limitations, the model reproduces an important hallmark of cardiac aging, namely QT prolongation.

Regarding drug effects in the ECG, drugs have conventionally been considered to have arrhythmogenic potential due to excessive prolongation of the QT/QTc interval if they prolong it by >20 ms, with an increase in the QTc of 10 ms being associated with a 5% increase in arrhythmic risk [63,64]. In our study, the adult models with ARIx below 25, which represent 65.95% of the population, show a median cisapride-induced QT prolongation of 22.42 ms, while the corresponding median prolongation in the SenesAge and AppAge populations is 31.64 and 32.69 ms, respectively, which suggests that age-related electrophysiological remodeling may itself contribute to increased risk, with an impact equal to or even greater than that of medium-risk drugs, and that drugs may exert larger effects in older individuals. Other ECG markers that have been associated with increased arrhythmic risk like Tpe [65] are found to be modestly higher in the BA population (Fig. 4**F,G**), thus supporting the need of further studying the electrophysiological remodeling related to age in humans and the inclusion of specific tests for vulnerable populations into the preclinical development of drugs.

In conclusion, the human-based methods developed in this study, which integrate human age-related transcriptomic data into *in silico* computational models, could be incorporated into the pipeline of preclinical drug safety assessment. Moreover, this approach may pave the way for similar projects targeting other organs where drug toxicity may differ between adult and older individuals, such as the renal system or the liver.

The authors declare no conflict of interest.

All relevant data are within the paper and its Supporting information files.

Ethics statement

This work is carried out with the highest ethical standards. No animal research nor human biological material or clinical data has been used in the study.

CRediT authorship contribution statement

Elisa Garrido-Huéscar: Writing – original draft, Software, Methodology, Formal analysis, Conceptualization. **Ricardo Maximiliano Rosales:** Writing – review & editing, Software, Methodology, Formal analysis. **María Pérez-Zabalza:** Writing – review & editing, Software, Methodology. **Pablo Laguna:** Writing – review & editing, Methodology, Investigation. **Laura Ordovás:** Writing – review & editing, Writing – original draft, Supervision, Investigation, Funding acquisition, Formal analysis, Conceptualization. **Esther Pueyo:** Writing – review & editing, Writing – original draft, Supervision, Software, Resources, Methodology, Investigation, Funding acquisition, Formal analysis, Conceptualization.

Declaration of competing interest

The authors declare that they have no known competing financial interests or personal relationships that could have appeared to influence the work reported in this paper.

Acknowledgements

This study was funded by projects PID2022-140556OB-I00 and PID2019-105674RB-I00 funded by MCIN/AEI/10.13039/501100011033/FEDER, UE, by project TED2021-130459B-I00 funded by MCIN/AEI/10.13039/501100011033, by the predoctoral grant CPT_09_19 and mobility grant MBV_04_23 funded by Gobierno de Aragón, the EMBO Scientific Exchange Grant 9907, PROY_B08_24 funded by Gobierno de Aragón, by ERC G.A. 638284 funded by European Research Council and by BSICoS group T39_23R funded by Aragón Government.

The Genotype-Tissue Expression (GTEx) Project was supported by the Common Fund of the Office of the Director of the National Institutes of Health, and by NCI, NHGRI, NHLBI, NIDA, NIMH, and NINDS. The bioinformatic analysis was carried out in collaboration with the Servicio de Biocomputación of the Instituto Aragonés de Ciencias de la Salud (IACS). Computations were performed using ICTS NANBIOSIS (High Performance Computing Unit at University of Zaragoza).

Supplementary materials

Supplementary material associated with this article can be found, in the online version, at doi:10.1016/j.cmpb.2026.109670.

References

[1] K.H. Lee, G.J. Kim, J.H. Kim, Correlation between drug market withdrawals and socioeconomic, health, and welfare indicators worldwide, J. Korean Med. Sci. 30 (2015) 1567–1576, https://doi.org/10.3346/jkms.2015.30.11.1567.

[2] N.S. Craveiro, B.S. Lopes, L. Tomás, S.F. Almeida, Drug withdrawal due to safety: a review of the data supporting withdrawal decision, Curr. Drug Saf. 15 (2019) 4–12, https://doi.org/10.2174/1574886314666191004092520.

[3] K. Kocadal, Drug-associated cardiovascular risks: a retrospective evaluation of withdrawn drugs, North. Clin. Istanb. 6 (2018) 196–202, https://doi.org/10.14744/nci.2018.44977.

[4] Z. Mou, P. Volarath, R. Racz, K.P. Cross, M. Girireddy, S. Chakravarti, L. Stavitskaya, Quantitative structure-activity relationship models to predict cardiac adverse effects, Chem. Res. Toxicol. 37 (2024) 1924–1933, https://doi.org/10.1021/acs.chemrestox.4c00186.

[5] P. Saxena, M.P. Hortigon-Vinagre, S. Beyl, I. Baburin, S. Andranovits, S.M. Iqbal, A. Costa, A.P. IJzerman, P. Kügler, E. Timin, G.L. Smith, S. Hering, Correlation between human ether-a-go-go-related gene channel inhibition and action potential prolongation, Br. J. Pharmacol. 174 (2017) 3081–3093, https://doi.org/10.1111/bph.13942.

[6] J. Shuren, International Conference on Harmonisation; guidance on E14 Clinical Evaluation of QT/QTc interval prolongation and proarrhythmic potential for non-antiarrhythmic drugs, Fed. Regist 70 (2005) 22–23.

[7] J. Brodsky, J. Shuren, International Conference on Harmonisation; guidance on S7B nonclinical evaluation of the potential for delayed ventricular repolarization (QT Interval Prolongation) by Human pharmaceuticals, Fed. Regist 70 (2005) 21–22.

[8] H.M. Vargas, A.S. Bass, J. Koerner, S. Matis-Mitchell, M.K. Pugsley, M. Skinner, M. Burnham, M. Bridgland-Taylor, S. Pettit, J.P. Valentin, Evaluation of drug-induced QT interval prolongation in animal and human studies: a literature review of concordance, Br. J. Pharmacol. 172 (2015) 4002–4011, https://doi.org/10.1111/bph.13207.

[9] CIPA Initiative. https://cipaproject.org/, 2013.

[10] O.J. Britton, A. Bueno-Orovio, L. Virág, A. Varró, B. Rodriguez, The electrogenic Na +/K+ pump is a key determinant of repolarization abnormality susceptibility in human ventricular cardiomyocytes: a population-based simulation study, Front. Physiol. 8 (2017) 1–13, https://doi.org/10.3389/fphys.2017.00278.

[11] J. Llopis-Lorente, J. Gomis-Tena, J. Cano, L. Romero, J. Saiz, B. Trenor, In silico classifiers for the assessment of drug proarrhythmicity, J. Chem. Inf. Model. 60 (2020) 5172–5187, https://doi.org/10.1021/acs.jcim.0c00201.

[12] Medicine use statistics, Eurostat (2022). https://ec.europa.eu/eurostat/statistics-explained/index.php?title=Medicine_use_statistics#Prescribed_medicines.
[13] E.D. Kantor, C.D. Rehm, J.S. Haas, A.T. Chan, E.L. Giovannucci, Trends in prescription drug use among adults in the United States from 1999 to 2012, JAMA - J. Am. Med. Assoc. 314 (2015) 1818–1831, https://doi.org/10.1001/jama.2015.13766.
[14] E.M. Screever, W.C. Meijers, J.J. Moslehi, Age-related considerations in cardio-oncology, J. Cardiovasc. Pharmacol. Ther. 26 (2021) 103–113, https://doi.org/10.1177/1074248420968689.
[15] D. García-Fuertes, E. Villanueva-Fernández, M. Crespín-Crespín, Drug-induced long-QT and torsades de pointes in elderly polymedicated patients, Arq. Bras. Cardiol. 106 (2016) 156–159, https://doi.org/10.5935/abc.20150069.
[16] European Medicences Agency, Annex III Amendments to the summaries of product characteristics and package leaflets, (2013) 4.
[17] S.W. Mittelstadt, N.A. Adams, R.D. Spruell, Age-dependent effects on cisapride-induced QTc prolongation in the isolated guinea pig heart, J. Pharmacol. Toxicol. Methods 54 (2006) 159–163, https://doi.org/10.1016/j.vascn.2006.02.011.
[18] E.M. Screever, W.C. Meijers, D.J. van Veldhuisen, R.A. de Boer, New developments in the pharmacotherapeutic management of heart failure in elderly patients: concerns and considerations, Expert Opin. Pharmacother. 18 (2017) 645–655, https://doi.org/10.1080/14656566.2017.1316377.
[19] N.A. Gude, K.M. Broughton, F. Firouzi, M.A. Sussman, Cardiac ageing: extrinsic and intrinsic factors in cellular renewal and senescence, Nat. Rev. Cardiol. 15 (2018) 523–542, https://doi.org/10.1038/s41569-018-0061-5.
[20] C. López-Otín, M.A. Blasco, L. Partridge, M. Serrano, G. Kroemer, Hallmarks of aging: an expanding universe, Cell 186 (2023) 243–278, https://doi.org/10.1016/j.cell.2022.11.001.
[21] F. Hatch, M.K. Lancaster, S.A. Jones, Aging is a primary risk factor for cardiac arrhythmias: disruption of intracellular Ca 2+ regulation as a key suspect, Expert Rev. Cardiovasc. Ther. 9 (2011) 1059–1067, https://doi.org/10.1586/erc.11.112.
[22] K. Saadeh, I.T. Fazmin, Mitochondrial dysfunction increases arrhythmic triggers and substrates; potential anti-arrhythmic pharmacological targets, Front. Cardiovasc. Med. 8 (2021) 1–17, https://doi.org/10.3389/fcvm.2021.646932.
[23] A. Biernacka, N.G. Frangogiannis, Aging and cardiac fibrosis, Aging Dis. 2 (2011) 158–173.
[24] A.A. Mangoni, M.T. Kinirons, C.G. Swift, S.H.D. Jackson, Impact of age on QT interval and QT dispersion in healthy subjects: a regression analysis, Age Ageing 32 (2003) 326–331, https://doi.org/10.1093/ageing/32.3.326.
[25] A.B. Curtis, R. Karki, A. Hattoum, U.C. Sharma, Arrhythmias in patients ≥80 years of age: pathophysiology, management, and outcomes, J. Am. Coll. Cardiol 71 (2018) 2041–2057, https://doi.org/10.1016/j.jacc.2018.03.019.
[26] A. Dokuchaev, S. Khamzin, O. Solovyova, In-silico study of age-related ionic remodeling in human ventricular cardiomyocytes, BIO Web. Conf. 22 (2020) 1024, https://doi.org/10.1051/bioconf/20202201024.
[27] N. Daily, J. Elson, T. Wakatsuki, Aging model for analyzing drug-induced proarrhythmia risks using cardiomyocytes differentiated from progeria-patient-derived induced pluripotent stem cells, Int. J. Mol. Sci. 24 (2023) 1–12, https://doi.org/10.3390/ijms241511959.
[28] E. Ramos-Marquès, L. García-Mendívil, M. Pérez-Zabalza, H. Santander-Badules, S. Srinivasan, J.C. Oliveros, R. Torres-Pérez, A. Cebollada, J.M. Vallejo-Gil, P. C. Fresneda-Roldán, J. Fañanás-Mastral, M. Vázquez-Sancho, M. Matamala-Adell, J.F. Sorribas-Berjón, J.A. Bellido-Morales, F.J. Mancebón-Sierra, A.S. Vaca-Núñez, C. Ballester-Cuenca, M. Jiménez-Navarro, J.M. Villaescusa, E. Garrido-Huéscar, M. Segovia-Roldán, A. Oliván-Viguera, C. Gómez-González, G. Muñiz, E. Diez, L. Ordovás, E. Pueyo, Chronological and biological aging of the human left ventricular myocardium: analysis of microRNAs contribution, Aging Cell 20 (2021) e13383, https://doi.org/10.1111/ACEL.13383.
[29] T. O'Hara, L. Virág, A. Varró, Y. Rudy, Simulation of the undiseased human cardiac ventricular action potential: model formulation and experimental validation, PLoS Comput. Biol. 7 (2011), https://doi.org/10.1371/journal.pcbi.1002061.
[30] Z. Li, B.J. Ridder, X. Han, W.W. Wu, J. Sheng, P.N. Tran, M. Wu, A. Randolph, R. H. Johnstone, G.R. Mirams, Y. Kuryshev, J. Kramer, C. Wu, W.J. Crumb, D. G. Strauss, Assessment of an In silico mechanistic model for proarrhythmia risk prediction under the CiPA initiative, Clin. Pharmacol. Ther. 105 (2019) 466–475, https://doi.org/10.1002/cpt.1184.
[31] M.D. McKay, R.J. Beckman, W.J. Conover, Comparison of three methods for selecting values of input variables in the analysis of output from a computer code, Technometrics 21 (1979) 239–245, https://doi.org/10.1080/00401706.1979.10489755.
[32] D.A. Sampedro-Puente, J. Fernandez-Bes, L. Virag, A. Varro, E. Pueyo, Data-driven identification of stochastic model parameters and State variables: application to the study of cardiac beat-to-beat variability, IEEE J. Biomed. Heal. Inform. 24 (2020) 693–704, https://doi.org/10.1109/jbhi.2019.2921881.
[33] S. Hamilton, D. Terentyev, Altered intracellular calcium homeostasis and arrhythmogenesis in the aged heart, Int. J. Mol. Sci. 20 (2019), https://doi.org/10.3390/ijms20102386.
[34] M.B. Sikkel, C. Hayward, K.T. MacLeod, S.E. Harding, A.R. Lyon, SERCA2a gene therapy in heart failure: an anti-arrhythmic positive inotrope, Br. J. Pharmacol. 171 (2014) 38–54, https://doi.org/10.1111/bph.12472.
[35] L.F. Shampine, M.W. Reichelt, The MATLAB ode suite, SIAM J. Sci. Comput. 18 (1997) 1–22, https://doi.org/10.1137/S1064827594276424.
[36] Z. Li, S. Dutta, J. Sheng, P.N. Tran, W. Wu, K. Chang, T. Mdluli, D.G. Strauss, T. Colatsky, Improving the in silico assessment of proarrhythmia risk by combining hERG (Human Ether-à-go-go-Related Gene) channel-drug binding kinetics and multichannel pharmacology, Circ. Arrhythmia Electrophysiol. 10 (2017) 1–12, https://doi.org/10.1161/CIRCEP.116.004628.
[37] C.E. Conrath, T. Opthof, Ventricular repolarization: an overview of (patho) physiology, sympathetic effects and genetic aspects, Prog. Biophys. Mol. Biol. 92 (2006) 269–307, https://doi.org/10.1016/j.pbiomolbio.2005.05.009.
[38] J.C. Gower, G.A.F. Seber, Multivariate observations, Biometrics 43 (1987) 478, https://doi.org/10.2307/2531831.
[39] D.A. Sampedro-Puente, J. Fernandez-Bes, B. Porter, S. Van Duijvenboden, P. Taggart, E. Pueyo, Mechanisms underlying interactions between low-frequency oscillations and beat-to-beat variability of celullar ventricular repolarization in response to sympathetic stimulation: implications for arrhythmogenesis, Front. Physiol. 10 (2019), https://doi.org/10.3389/fphys.2019.00916.
[40] K.H.W.J. Ten Tusscher, A.V. Panfilov, Alternans and spiral breakup in a human ventricular tissue model, Am. J. Physiol. - Hear. Circ. Physiol. 291 (2006) 1088–1100, https://doi.org/10.1152/ajpheart.00109.2006.
[41] S. Dutta, A. Mincholé, T.A. Quinn, B. Rodriguez, Electrophysiological properties of computational human ventricular cell action potential models under acute ischemic conditions, Prog. Biophys. Mol. Biol. 129 (2017) 40–52, https://doi.org/10.1016/j.pbiomolbio.2017.02.007.
[42] M.M. Elshrif, E.M. Cherry, A quantitative comparison of the behavior of human ventricular cardiac electrophysiology models in tissue, PLoS. One 9 (2014), https://doi.org/10.1371/journal.pone.0084401.
[43] K.A. Mountris, E. Pueyo, The radial point interpolation mixed collocation method for the solution of transient diffusion problems, Eng. Anal. Bound. Elem. 121 (2020) 207–216, https://doi.org/10.1016/j.enganabound.2020.10.005.
[44] K.A. Mountris, E. Pueyo, A dual adaptive explicit time integration algorithm for efficiently solving the cardiac monodomain equation, Int. J. Numer. Method. Biomed. Eng. 37 (2021) 1–11, https://doi.org/10.1002/cnm.3461.
[45] C. Pérez, R. Cebollada, K.A. Mountris, J.P. Martínez, P. Laguna, E. Pueyo, The role of β-adrenergic stimulation in QT interval adaptation to heart rate during stress test, PLoS. One 18 (2023) 1–22, https://doi.org/10.1371/journal.pone.0280901.
[46] J.P. Martínez, R. Almeida, S. Olmos, A.P. Rocha, P. Laguna, A wavelet-based ECG delineator evaluation on standard databases, IEEE Trans. Biomed. Eng. 51 (2004) 570–581, https://doi.org/10.1109/TBME.2003.821031.
[47] M.-F. Wang, C. Hou, F. Jia, C.-H. Zhong, C. Xue, J.-J. Li, Aging- associated atrial fibrillation: a comprehensive review focusing on the potential mechanisms, Aging Cell 23 (2024) 1–22, https://doi.org/10.1111/acel.14309.
[48] E.L. Holmuhamedov, P. Chakraborty, A. Oberlin, X. Liu, M. Yousufuddin, W. K. Shen, A. Terzic, A. Jahangir, Aging-associated susceptibility to stress-induced ventricular arrhythmogenesis is attenuated by tetrodotoxin, Biochem. Biophys. Res. Commun. 623 (2022) 44–50, https://doi.org/10.1016/j.bbrc.2022.07.040.
[49] H.A. Feridooni, K.M. Dibb, S.E. Howlett, How cardiomyocyte excitation, calcium release and contraction become altered with age, J. Mol. Cell. Cardiol. 83 (2015) 62–72, https://doi.org/10.1016/j.yjmcc.2014.12.004.
[50] H.-M. Su, H.-C. Chiu, T.-H. Lin, W.-C. Voon, H.W. Liu, W.-T. Lai, Longitudinal study of the ageing trends in QT interval and dispersion in healthy elderly subjects, Age Ageing 35 (2006) 636–638, https://doi.org/10.1093/ageing/afl114.
[51] A.S. Vink, S.A.B. Clur, A.A.M. Wilde, N.A. Blom, Effect of age and gender on the QTc-interval in healthy individuals and patients with long-QT syndrome, Trends Cardiovasc. Med. 28 (2018) 64–75, https://doi.org/10.1016/j.tcm.2017.07.012.
[52] P.K. Gupta, Principles and basic concepts of toxicokinetics, Fundam. Toxicol. (2016) 87–107, https://doi.org/10.1016/B978-0-12-805426-0.00009-3.
[53] J. Walmsley, J.F. Rodriguez, G.R. Mirams, K. Burrage, I.R. Efimov, B. Rodriguez, mRNA expression levels in failing Human hearts predict cellular electrophysiological remodeling: a population-based simulation study, PLoS. One 8 (2013), https://doi.org/10.1371/journal.pone.0056359.
[54] M. Moqri, C. Herzog, J.R. Poganik, J. Justice, D.W. Belsky, A. Higgins-Chen, A. Moskalev, G. Fuellen, A.A. Cohen, I. Bautmans, M. Widschwendter, J. Ding, A. Fleming, J. Mannick, J.D.J. Han, A. Zhavoronkov, N. Barzilai, M. Kaeberlein, S. Cummings, B.K. Kennedy, L. Ferrucci, S. Horvath, E. Verdin, A.B. Maier, M. P. Snyder, V. Sebastiano, V.N. Gladyshev, Biomarkers of aging for the identification and evaluation of longevity interventions, Cell 186 (2023) 3758, https://doi.org/10.1016/J.CELL.2023.08.003.
[55] K.M. Keller, S.E. Howlett, Sex differences in the biology and pathology of the aging heart, Can. J. Cardiol 32 (2016) 1065–1073, https://doi.org/10.1016/j.cjca.2016.03.017.
[56] M. Bencurova, T. Lysikova, K. Leskova Majdova, P. Kaplan, P. Racay, J. Lehotsky, Z. Tatarkova, Age-dependent changes in calcium regulation after myocardial ischemia–Reperfusion injury, Biomedicines 11 (2023), https://doi.org/10.3390/biomedicines11041193.
[57] B.S. Cain, D.R. Meldrum, K.S. Joo, J.F. Wang, X. Meng, J.C. Cleveland, A. Banerjee, A.H. Harken, Human SERCA2a levels correlate inversely with age in senescent human myocardium, J. Am. Coll. Cardiol. 32 (1998) 458–467, https://doi.org/10.1016/S0735-1097(98)00233-2.
[58] Y.Y. Zhou, E.G. Lakatta, R.P. Xiao, Calcium cycling in the aged heart, Asia Pac. Hear. J. 8 (1999) 88–96, https://doi.org/10.1016/S1328-0163(99)90070-2.
[59] C. Hawkins, A. Xu, N. Narayanan, Sarcoplasmic reticulum calcium pump in cardiac and slow twitch skeletal muscle but not fast twitch skeletal muscle undergoes phosphorylation by endogenous and exogenous Ca2+/calmodulin-dependent protein kinase: characterization of optimal conditions for c, J. Biol. Chem. 269 (1994) 31198–31206, https://doi.org/10.1016/s0021-9258(18)47409-1.
[60] M.S. Salahudeen, P.S. Nishtala, An overview of pharmacodynamic modelling, ligand-binding approach and its application in clinical practice, Saudi Pharm. J. 25 (2017) 165–175, https://doi.org/10.1016/j.jsps.2016.07.002.

[61] M. Sagiv, E. Goldhammer, D. Ben-Sira, R. Amir, Factors defining oxygen uptake at peak exercise in aged people, Eur. Rev. Aging Phys. Act. 7 (2010) 1–2, https://doi.org/10.1007/s11556-010-0061-x.

[62] L. García-Mendívil, M. Pérez-Zabalza, K. Mountris, S. Duwé, N. Smisdom, M. Pérez, L. Luján, E. Wolfs, R.B. Driesen, J.M. Vallejo-Gil, P.C. Fresneda-Roldán, J. Fañanás-Mastral, M. Vázquez-Sancho, M. Matamala-Adell, J.F. Sorribas-Berjón, J.A. Bellido-Morales, F.J. Mancebón-Sierra, A.S. Vaca-Núñez, C. Ballester-Cuenca, A. Oliván-Viguera, E. Diez, L. Ordovás, E. Pueyo, Analysis of age-related left ventricular collagen remodeling in living donors: implications in arrhythmogenesis, iScience (2022) 25, https://doi.org/10.1016/j.isci.2022.103822.

[63] R. Khatib, F.R.N. Sabir, C. Omari, C. Pepper, M.H. Tayebjee, Managing drug-induced QT prolongation in clinical practice, Postgr. Med. J. 97 (2021) 452–458, https://doi.org/10.1136/postgradmedj-2020-138661.

[64] M.I. Then, W. Andrikyan, R. Maas, M.F. Fromm, The CredibleMeds® list: usage of QT interval prolonging drugs in Germany and discordances with prescribing information, Br. J. Clin. Pharmacol. 88 (2022), https://doi.org/10.1111/bcp.14951.

[65] U.M.R. Avula, L. Melki, J.S. Kushner, S. Liang, E.Y. Wan, Theoretical models and computational analysis of action potential dispersion for cardiac arrhythmia risk stratification, Front. Cardiovasc. Med. 8 (2021) 1–8, https://doi.org/10.3389/fcvm.2021.649489.